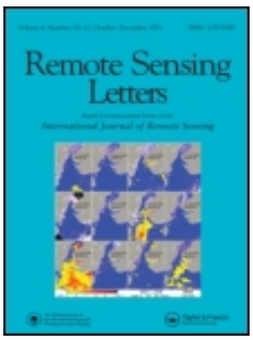

Remote Sensing Letters

ISSN: 2150-704X (Print) 2150-7058 (Online) Journal homepage: http://www.tandfonline.com/loi/trsl20

Fusion-based approach to change detection to reduce the effect of the trade-off parameter in the active contour model

Ming Hao, Wenzhong Shi, Kazhong Deng & Hua Zhang

To cite this article: Ming Hao, Wenzhong Shi, Kazhong Deng & Hua Zhang (2015) Fusion-based approach to change detection to reduce the effect of the trade-off parameter in the active contour model, Remote Sensing Letters, 6:1, 39-48, DOI: 10.1080/2150704X.2014.1001078

To link to this article: http://dx.doi.org/10.1080/2150704X.2014.1001078

Published online: 08 Jan 2015.

Remote Sensing Letters, 2015
Vol. 6, No. 1, 39–48, http://dx.doi.org/10.1080/2150704X.2014.1001078

Taylor & Francis
Taylor & Francis Group

Fusion-based approach to change detection to reduce the effect of the trade-off parameter in the active contour model

Ming Hao[a], Wenzhong Shi[b]*, Kazhong Deng[a], and Hua Zhang[a]

[a]*School of Environment Science and Spatial Informatics, China University of Mining and Technology, Xuzhou, China;* [b]*Joint Research Laboratory on Spatial Information, The Hong Kong Polytechnic University and Wuhan University, Hong Kong and Wuhan, China*

(*Received 18 June 2014; accepted 16 December 2014*)

This study proposes an approach to unsupervised change detection in which two different change maps are fused using different trade-off parameters of an active contour model. First, the change vector analysis method is conducted to produce a difference image from multitemporal and multispectral remotely sensed images. Second, two change maps are obtained based on the difference image using an active contour model using two different values of the trade-off parameter. Finally, an advantage fusion strategy is proposed to yield a final change map by fusing the two change maps, thereby reducing false alarms and preserving the accurate outlines of the changed regions. Two experiments are conducted with Landsat-7 Enhanced Thematic Mapper Plus and Landsat-5 Thematic Mapper data sets to evaluate the performance of the proposed method. Results confirm the effectiveness of the proposed approach vis-à-vis some of the state-of-the-art methods. This work contributes to the reduction of the effect of the trade-off parameter on the accuracy of the change map.

1. Introduction

Change detection aims to identify changes by analysing multitemporal remotely sensed images acquired in the same geographical area at different times (Lu et al. 2004). Change detection methods can generally be grouped into supervised (i.e., post-classification) and unsupervised types.

The unsupervised methods include image differencing, image ratioing, image regression, principal component analysis, and change vector analysis (CVA) (Lu et al. 2004). Other methods based on pattern recognition and context information are also developed by further processing the difference image generated using image differencing or CVA. The active contour model is one such method that has been applied to change detection in recent years. This model was proposed by Kass, Witkin, and Terzopoulos (1988) and was improved by Chan and Vese (2001) as the Chan–Vese (CV) model, in which a level set was used to detect objects without boundaries defined by a gradient. Given its implicit handling of topological changes and low sensitivity to noise, the CV model has gained popularity in the field of change detection through remote sensing images (Bazi, Melgani, and Al-Sharari 2010; Shi and Hao 2013; Li, Gong, and Liu 2015). Bazi, Melgani, and Al-Sharari (2010) developed the multiresolution level set (MLS) and MLS with the Kittler algorithm (MLSK) methods based on an active contour model to detect changes using multitemporal remote sensing images. Wavelet transform was adopted to reduce the noise of difference images, and the active contour model was then integrated to detect changes based on the transformed images (Celik and Ma 2011; Chen and Cao 2013). Cao, Liu, and

*Corresponding author. Email: lswzshi@polyu.edu.hk

Shang (2014) incorporated neighbourhood constraints into the active contour model to reduce the noise and smooth boundaries of the changed regions. Hao et al. (2014) proposed an expectation–maximization (EM)-based active contour model using a level set to generate robust results for different changes. Fuzzy active contour models were developed to enhance the change information and reduce the effect of speckle noise using local information and fuzzy sets (Shi et al. 2014; Li, Gong, and Liu 2015). The active contour model was also implemented to extract inhomogeneous insulators from aerial images by exploiting texture information, which is similar to the extraction of changes (Wu and An 2014). However, a trade-off parameter is required to control the trade-off between the goodness of fit and the length of the contour in the active contour model. On the one hand, when the trade-off parameter is small, the results contain many false alarms. On the other hand, the change map may lose some detailed changes (i.e., small changes and accurate boundaries of the changed regions) under a large trade-off parameter (Bazi, Melgani, and Al-Sharari 2010; Hao et al. 2014; Li, Gong, and Liu 2015). Framed by this context, the present study proposes an approach to change detection in which two change maps are fused using different trade-off parameters of the active contour model with a level set to reduce the effect of the trade-off parameter on the accuracy of the change maps.

The proposed approach mainly consists of three steps: First, CVA is conducted on multitemporal images to generate a difference image. Second, the CV model obtains two change maps using two different trade-off parameters. Finally, the two change maps are fused to generate the final change map. In this step, an advantage fusion strategy is suggested at the feature level to achieve a satisfactory trade-off between reducing false alarms and retaining detailed changes. Experiments are conducted on two data sets to assess the effectiveness of the proposed approach.

2. Proposed approach to change detection

We suppose that two multispectral images, $\mathbf{X}_1 = \{x_1^l(i,j)|1 \le i \le m,\ 1 \le j \le n,\ 1 \le l \le L\}$ and $\mathbf{X}_2 = \{x_2^l(i,j)|1 \le i \le m,\ 1 \le j \le n,\ 1 \le l \le L\}$, of size $m \times n$ pixels and consisting of L bands are acquired from the same geographical area at two different times. Considering that the focus is on the change detection process, the images are assumed to have been co-registered and radiometrically corrected. Let $\mathbf{X}$ be the difference image of size $m \times n$ generated from $\mathbf{X}_1$ and $\mathbf{X}_2$ using the CVA technique. The image $\mathbf{X}_1$ is subtracted from the image $\mathbf{X}_2$ to produce a change vector image, and their modulus is computed as the difference image (Bazi, Melgani, and Al-Sharari 2010).

2.1. *Producing initial change maps using the active contour model*

One of the most well-known active contour models, the CV model is a region-based segmentation algorithm. The difference image $\mathbf{X}$ can be segmented into changed and unchanged parts when an optimal contour C is found by minimizing the energy function as follows (Chan and Vese 2001):

$$E(\mathrm{C}, c_1, c_2) = \int_{\mathrm{I(C)}} |X(x,y) - c_1|^2 \mathrm{d}x\mathrm{d}y + \int_{\mathrm{O(C)}} |X(x,y) - c_2|^2 \mathrm{d}x\mathrm{d}y + \mu|\mathrm{C}|, \tag{1}$$

where C is the evolving contour, $X(x,y)$ is the grey value of the pixel at location (x,y), I(C) represents the area inside the evolving contour, O(C) denotes the area outside the evolving contour, $\mu > 0$ is a constant trade-off parameter and controls the trade-off between the fitness and the length of the contour C, |C| denotes the length of the evolving contour, and c_1 and c_2 are the mean grey values of all pixels inside and outside the contour C, respectively.

The level set method of Osher and Sethian (1988) is exploited to minimize the energy function (1). The contour C is represented by a zero level set of function ϕ over the difference image, such that

$$\begin{cases} \phi(x,y) > 0 & (x,y) \in I(\mathrm{C}) \\ \phi(x,y) = 0 & (x,y) \in \mathrm{C} \\ \phi(x,y) < 0 & (x,y) \in O(\mathrm{C}) \end{cases}. \tag{2}$$

The Heaviside function H and Dirac delta function δ are used and, respectively, defined as

$$H(z) = \begin{cases} 1 & z \geq 0 \\ 0 & z < 0 \end{cases}, \quad \delta(z) = \frac{\mathrm{d}}{\mathrm{d}z} H(z). \tag{3}$$

Equation (1) can be rewritten by replacing the unknown variable C with the level set ϕ using Equation (3) as follows:

$$\begin{aligned} E(\phi, c_1, c_2) = & \int_\Omega |X(x,y) - c_1|^2 H(\phi(x,y)) \mathrm{d}x\mathrm{d}y + \int_\Omega |X(x,y) - c_2|^2 [1 - H(\phi(x,y))] \mathrm{d}x\mathrm{d}y \\ & + \mu \int_\Omega \delta(\phi(x,y)) |\nabla \phi(x,y)| \mathrm{d}x\mathrm{d}y \end{aligned}, \tag{4}$$

where Ω represents a given image. The energy function is minimized with respect to ϕ when c_1 and c_2 are kept constant. The parameters c_1 and c_2 can be expressed as

$$c_1 = \frac{\int_\Omega X(x,y) H(\phi(x,y)) \mathrm{d}x\mathrm{d}y}{\int_\Omega H(\phi(x,y)) \mathrm{d}x\mathrm{d}y}, \quad c_2 = \frac{\int_\Omega X(x,y) [1 - H(\phi(x,y))] \mathrm{d}x\mathrm{d}y}{\int_\Omega [1 - H(\phi(x,y))] \mathrm{d}x\mathrm{d}y}. \tag{5}$$

Using the gradient descent method, the Euler–Lagrange equation for ϕ, parameterizing the descent direction by an artificial time t ($t \geq 0$) is given by

$$\frac{\partial \phi}{\partial t} = \delta(\phi) \left[\mu \, \mathrm{div}\left(\frac{\nabla \phi}{|\nabla \phi|} \right) - |X(x,y) - c_1|^2 + |X(x,y) - c_2|^2 \right]. \tag{6}$$

A finite difference implicit scheme is then exploited to discretize this equation and achieve the solution to the evolution equation in ϕ. We refer the reader to Chan and Vese (2001) for more details on numerical approximation. The contour C then partitions the difference image into the changed and unchanged parts when the energy function reaches its minimum.

2.2. *Advantage fusion of different change maps*

Given that the trade-off parameter μ controls the trade-off between the fitness and the length of the contour C, the values of μ greatly affect the accuracy of the change maps. Hence, a fusion strategy is proposed in this section to reduce the effect of the trade-off parameter μ on the final change map. In this fusion strategy, two different values of μ – a small value, μ_s, and a large value, μ_l – are adopted to produce two different change maps $\mathbf{M}_s$ and $\mathbf{M}_l$. A small μ_s results in accurate outlines of changed regions but simultaneously produces many false alarms. However, a large μ_l not only removes some false alarms but also loses accurate outlines of changed regions. Therefore, the advantages of different level change maps $\mathbf{M}_s$ and $\mathbf{M}_l$ are considered in the fusion strategy to generate a final

change map $\mathbf{M}_f$ with accurate outlines of changed regions and a few false alarms. The detailed process is presented as follows.

Step 1: The independent changed regions in $\mathbf{M}_s$ are labelled as clusters $C_s = \{C_s^1, C_s^2, \ldots, C_s^p\}$, and the changed regions in $\mathbf{M}_l$ are labelled as clusters $C_l = \{C_l^1, C_l^2, \ldots, C_l^q\}$ for the connected components with four connected pixels, as shown in Figure 1(*a*). Figures 1(*b*) and (*c*) represent the change maps $\mathbf{M}_s$ and $\mathbf{M}_l$, the three clusters with detailed information are labelled as C_s^1, C_s^2, C_s^3, and the only cluster containing coarse but less false change information is labelled as C_l^1.

Step 2: The change map $\mathbf{M}_l$ is used to refine the change map $\mathbf{M}_s$. If

$$C_s^i \cap C_l^j \neq \varnothing \quad (1 \leq i \leq p,\ 1 \leq j \leq q), \tag{7}$$

then C_s^i is treated as true changes and is retained in the final change map $\mathbf{M}_f$, where C_s^i and C_l^i are the *i*-th labelled cluster in the change maps $\mathbf{M}_s$ and $\mathbf{M}_l$, respectively. If any pixel of the change cluster C_s^i is also identified as changed in $\mathbf{M}_l$, this cluster therefore belongs to the true changes. Figure 1 shows that the clusters C_s^1 and C_s^2 in $\mathbf{M}_s$ include the same pixels as those of cluster C_l^1 in $\mathbf{M}_l$. Hence, they are retained in the final change map. If

$$C_s^i \cap C_l^j = \varnothing \quad (1 \leq i \leq p,\ 1 \leq j \leq q), \tag{8}$$

then C_s^i is treated as noise and is removed from the final change map $\mathbf{M}_f$. Given that the cluster C_s^3 of Figure 1(*b*) has no overlapping pixel with the cluster C_l^1 of Figure 1(*c*), it is assumed as noise and is removed from the final change map of Figure 1(*d*). The cluster C_l^i is used to confirm C_s^i change because $\mathbf{M}_l$ removes much false alarms, and the main changed regions are retained. The cluster C_s^i is treated as the true changes and is retained in the final change map when C_s^i intersects with C_l^i because C_s^i contains the accurate edges and outlines of the changed regions, unlike C_l^i. As such, both advantages of $\mathbf{M}_s$ and $\mathbf{M}_l$ are considered and preserved in the fused change map.

Step 3: After all the clusters of $\mathbf{M}_s$ are checked and fused with $\mathbf{M}_l$ via step 2, the final change map $\mathbf{M}_f$ is obtained. Figures 1(*e*) and (*f*) show that some pixels of the clusters

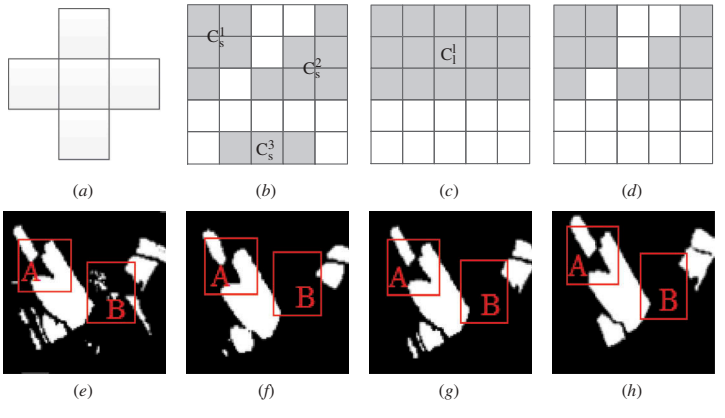

Figure 1. (*a*) Four connected pixels; examples of simulated change maps (*b*) $\mathbf{M}_s$, (*c*) $\mathbf{M}_l$, (*d*) $\mathbf{M}_f$; examples of real change maps (*e*) $\mathbf{M}_s$, (*f*) $\mathbf{M}_l$, (*g*) $\mathbf{M}_f$, and (*h*) the reference. The rectangles A and B show the abilities of the proposed method to retain detailed changes and remove false alarms, respectively.

of region A in $\mathbf{M}_s$ are also identified as changed in $\mathbf{M}_l$, and all pixels of the clusters of region B in $\mathbf{M}_s$ are detected as unchanged in $\mathbf{M}_l$. Therefore, the clusters of region A in $\mathbf{M}_s$ are retained, and the clusters of region B in $\mathbf{M}_s$ are removed in the final change map $\mathbf{M}_f$, as shown in Figure 1(*g*).

3. Experimental results and discussion

3.1. Description of the data set

Two data sets were used in the experiments to assess the effectiveness of the proposed approach to change detection. The first data set (300 × 280 pixels) was acquired by the Landsat-7 Enhanced Thematic Mapper Plus (ETM+) sensor in August 2001 and 2002 in Northeast China. The second data set (700 × 650 pixels) was acquired by Landsat-5 Thematic Mapper (TM) in August 2007 and 2010 in Northeast China. The difference images were generated using the CVA technique from all the bands, except for the thermal infrared band (band 6). Figure 2 shows the multitemporal images and the difference images of the data sets.

To quantitatively evaluate the performance of the proposed approach for change detection, five indices were used to assess the results for all pixels (Yetgin 2012): (1) missed detections, (2) false alarms, (3) total errors, (4) kappa coefficient, and (5) improved percentage of total errors (IPTE). IPTE can be calculated as $((T_b - T_a)/T_b) \times 100\%$, where T_a and T_b are the total errors of the proposed method and a comparative method, respectively. The reference change maps were created through the visual analysis of the input images based on the multitemporal images of the two data sets.

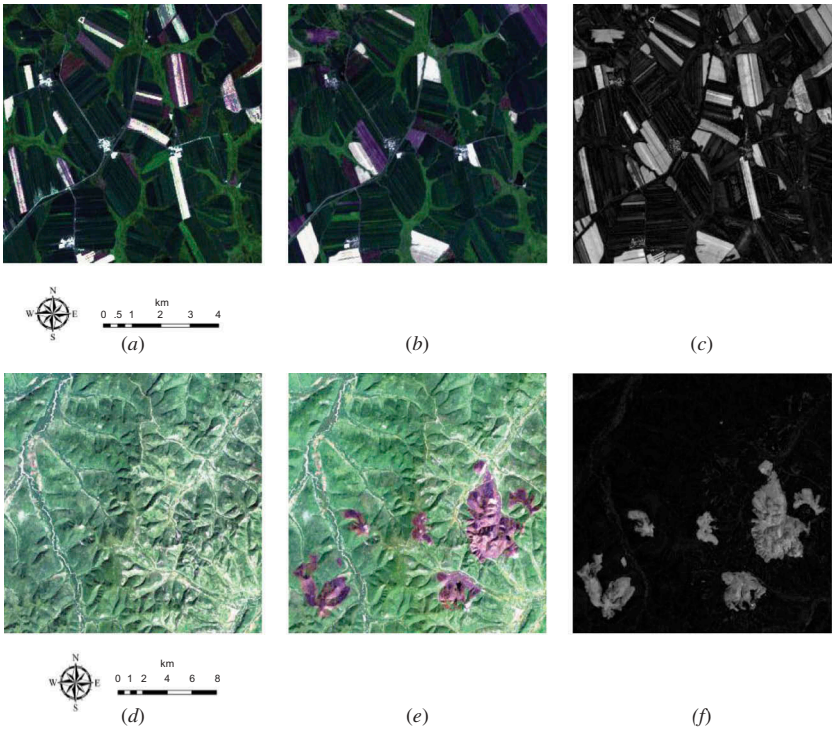

Figure 2. (*a*) August 2001, (*b*) August 2002, and (*c*) the difference image of data set 1 (the centre coordinate: 48°3′ N, 126°8′ E); (*d*) August 2007, (*e*) August 2010, and (*f*) the difference image of data set 2 (the centre coordinate: 51°6′ N, 123°1′ E).

3.2. Experimental results of data set 1

Several experiments were conducted on data set 1. The same convergence criterion was adopted, and the number of iterations for the level set of all the methods used in this study was fixed to 200. First, the CV model was implemented, and different values of the trade-off parameter μ ranging from 0 to 1.1 with a step of 0.1 were used to generate the change maps. Some change maps are shown in Figure 3. The false alarms were evidently reduced, and more completely changed regions were detected as the μ value increased. However, detailed changes were missing relative to the reference change map. This phenomenon was mainly caused by the parameter μ of the active contour model, which controls the trade-off between the goodness of fit and the length of the curve C.

The change maps generated by the μ values of 0.2 and 1.0 were then selected and fused using the proposed advantage fusion strategy. The fused change map is displayed in Figure 3(*f*). The rectangular boxes in Figure 3 show that the change map of the μ value of 0.2 reached the satisfactory outlines of the changed regions but contained some false alarms. Conversely, the change map of the μ value of 1 had minimal false alarms but had smoothed outlines of the changed regions. However, the false alarms were reduced in the fused change map. The outlines of the changed regions were also accurately detected. More accurate changed regions were eventually obtained through the fusion method because the advantages of the results yielded by the small and large μ values were fused at the feature level. Figure 4 presents the *variations* in the missed detections, false alarms, and total errors when different μ values are used in the CV model and proposed method. In the proposed method, the change map generated by the μ value of 0.2 was fused with different change maps using the μ value ranging from 0 to 1.1. All the missed detections, false alarms, and total errors of the CV model

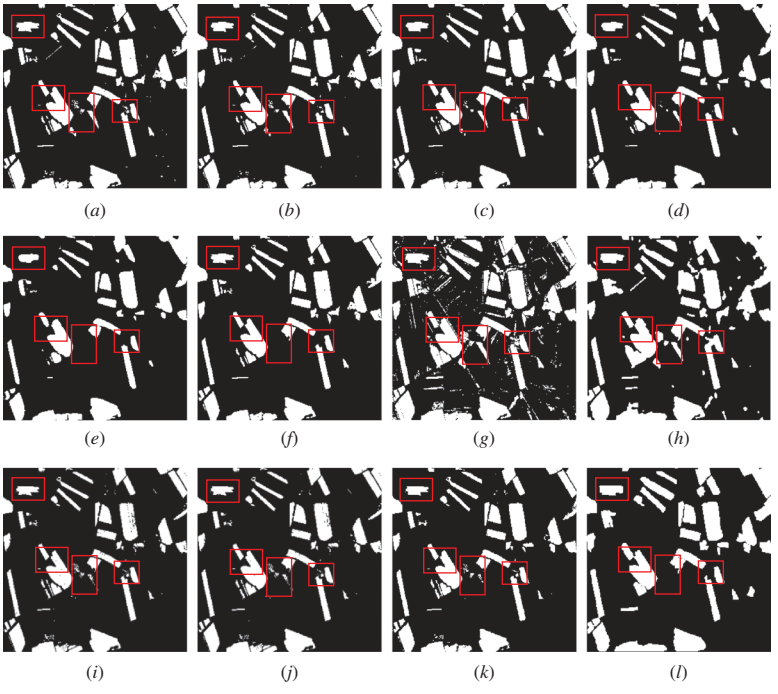

Figure 3. Change maps of data set 1 generated by the active contour model using μ values of (*a*) 0.2, (*b*) 0.4, (*c*) 0.6, (*d*) 0.8, and (*e*) 1.0; change map (*f*) was generated using the proposed fusion method with μ values of 0.2 and 1.0; change maps (*g*), (*h*), (*i*), (*j*), and (*k*) generated by EM, MRF (β = 1.8), MLS (μ = 0.2), MLSK (μ = 0.2), and UDWTAC (μ = 0.1); (*l*) is the reference.

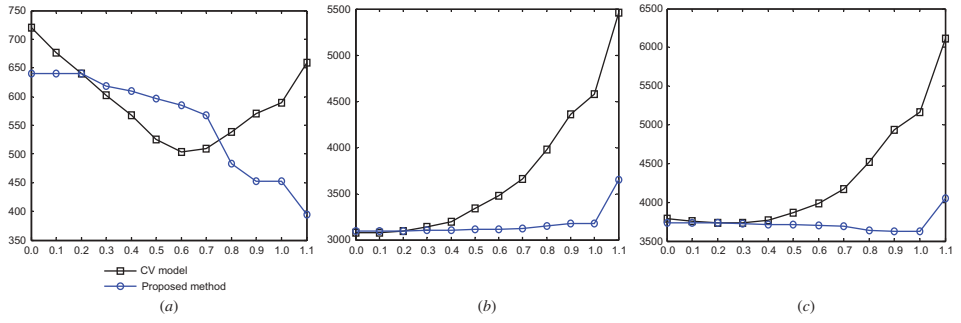

Figure 4. Variations in (*a*) false alarms, (*b*) missed detections, and (*c*) total errors of the CV model and proposed method when the change map generated by the μ value of 0.2 was fused with another change map generated by μ values ranging from 0 to 1.1 with a step of 0.1 for data set 1.

first dropped and then increased as the μ value increased. For the proposed method, as the μ value increased, the false alarms continuously decreased, and the missed detections slightly increased. The total errors generally dropped and reached the minimum at the μ value of 1.

Several further comparisons were also conducted with the CV model, EM-based threshold method, Markov random field (MRF) method (Bruzzone and Prieto 2000), MLS, MLSK, and undecimated discrete wavelet transform and active contour (UDWTAC) approach (Celik and Ma 2011). The β value of MRF was set to 1.8, which is a constant that tunes the influence of the spatial-contextual information. The μ values of CV, MLS, and MLSK were all set to 0.2, and the μ value of UDWTAC was set to 0.1 to produce change maps, as shown in Figure 3. The proposed approach produced the most accurate change map among all the methods; more details on their accuracy can be found in Table 1. The total errors were reduced by 42.3%, 26.4%, 4.4%, 4.7%, 3.9%, and 4.6% for the EM, MRF, CV, MLS, MLSK, and UDWTAC methods, respectively.

3.3. *Experimental results of data set 2*

Experiments were also conducted on data set 2. The same convergence criterion was adopted, and the number of iterations for the level set of all the methods used in this study was fixed to 200. Figure 5 shows parts of the change maps generated by the CV model using μ values ranging from 0 to 1.1 with a step of 0.1. Detailed changes were detected when the μ value was small. However, many false alarms were found in these change maps. Afterward, the false alarms decreased with an increase in the μ value, but excessively smooth changes were obtained.

The fused change map shown in Figure 5(*f*) was fused from two change maps generated by the μ values of 0.2 and 1.0. The false alarms were reduced, and detailed changes were accurately detected, as marked by the rectangles of Figure 5(*f*). The variations in the three indices (i.e., missed detections, false alarms, and total errors) when different μ values are used

Table 1. Quantitative comparison of data set 1 using the comparative and proposed methods.

Methods	False alarms (no. of pixels)	Missed detections (no. of pixels)	Total errors (no. of pixels)	Kappa coefficient	IPTE (%)
EM	5420	863	6283	0.7851	42.3
MRF	4202	725	4927	0.8276	26.4
CV	640	3099	3739	0.8502	4.4
MLS	722	3086	3808	0.8478	4.7
MLSK	721	3054	3775	0.8492	3.9
UDWTAC	612	3191	3803	0.8472	4.6
Proposed method	452	3176	3628	0.8537	–

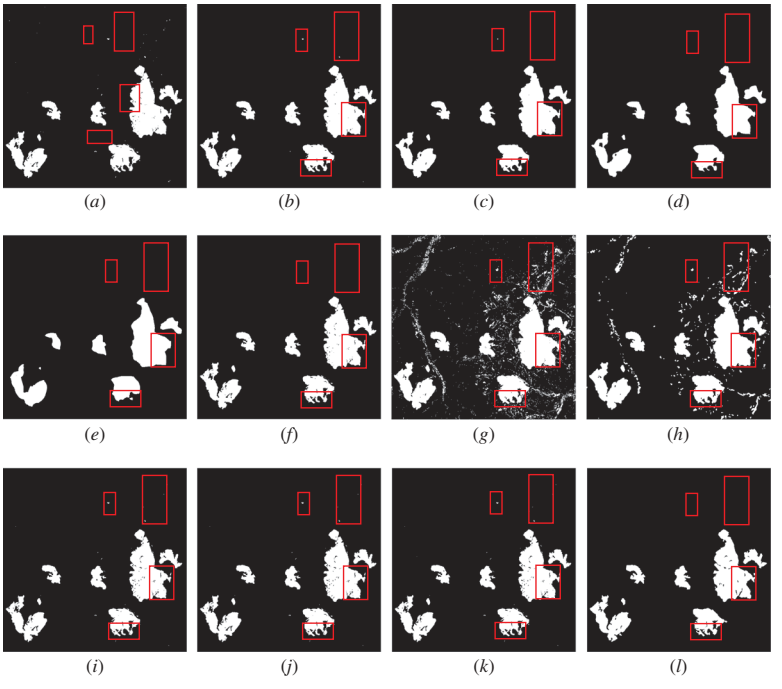

Figure 5. Change maps of data set 2 generated by the active contour model using μ values of (*a*) 0.2, (*b*) 0.4, (*c*) 0.6, (*d*) 0.8, and (*e*) 1.0; change map (*f*) was generated by the proposed fusion method with μ values of 0.2 and 1.0; change maps (*g*), (*h*), (*i*), (*j*), and (*k*) generated by EM, MRF (β = 1.5), MLS (μ = 0.2), MLSK (μ = 0.2), and UDWTAC (μ = 0.2); (*l*) is the reference.

in the CV model and proposed method are shown in Figure 6. In the proposed method, the change map generated by the μ value of 0.2 was fused with different change maps produced by μ values ranging from 0 to 1.1 with a step of 0.1. All the three indices of the CV model first dropped and then increased as the μ value increased. For the proposed method, the false alarms always decreased with an increase in the value of μ, while the missed detections were nearly constant. As a result, the total errors declined and reached the minimum when the change map generated by the μ value of 1 was used for fusion. When the false alarms of the CV model increased, those of the proposed method still dropped because the process of reducing false alarms occurred at the feature level rather than the pixel level.

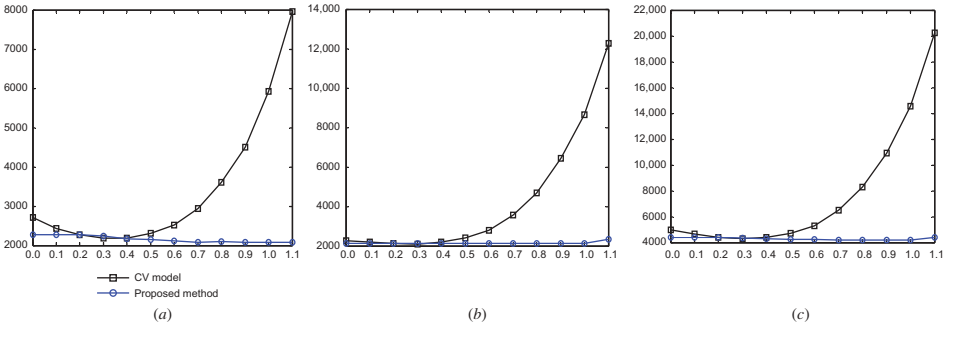

Figure 6. Variations in (*a*) false alarms, (*b*) missed detections, and (*c*) total errors of the CV model and proposed method when the change map generated by the μ value of 0.2 was fused with another change map generated by μ values ranging from 0 to 1.1 with a step of 0.1 for data set 2.

Table 2. Quantitative comparison of data set 2 using the comparative and proposed methods.

Methods	False alarms (no. of pixels)	Missed detections (no. of pixels)	Total errors (no. of pixels)	Kappa coefficient	IPTE (%)
EM	21,922	446	22,368	0.7800	81.3
MRF	15,435	319	15,754	0.8370	73.4
CV	2270	2109	4379	0.9483	4.2
MLS	2279	2366	4645	0.9451	9.7
MLSK	2279	2363	4642	0.9451	9.7
UDWTAC	2297	2371	4668	0.9448	10.2
Proposed method	2084	2110	4194	0.9504	–

Several change detection methods were implemented, such as EM, MRF, CV, MLS, MLSK, and UDWTAC. The β value of MRF was set to 1.5, and all the μ values of CV, MLS, MLSK, and UDWTAC were set to 0.2 to produce change maps, as shown in Figure 5. Table 2 illustrates the quantitative results obtained by all the change detection methods used in this study; the total errors were reduced by 81.3%, 73.4%, 4.2%, 9.7%, 9.7%, and 10.2%. The proposed technique produced the most accurate change map among all the techniques used in this study.

Two trade-off parameters are needed in the fusion strategy. If they are too close to each other, a significant improvement cannot be obtained. However, if the values of the two trade-off parameters are too different, the problem of missed detections may occur. In this study, the value of the small trade-off parameter μ was set to 0.2 because this value results in relatively accurate outlines and minimal missed detections, as indicated in the literature. The value of the large μ was empirically set to 1.0, and the experiments on the different data sets indicated that this value generates satisfactory results. When the changed regions are small and have relatively small values in the difference image, these regions may be missed by the proposed fusion rule because they may be detected as unchanged using a relatively larger μ. The proposed method mostly decreases the false alarms and keeps missed detections nearly constant. Considering that CV, MLS, MLSK, and UDWTAC are efficient methods of change detection and always generate accurate change maps, the improvements of the proposed method are not significant. Nevertheless, the proposed method reduces the effect of trade-off parameter in the active contour model to some extent. The experimental results also indicate that the proposed approach is competitive and often performs more accurately than the other approaches used in this study in terms of total errors, kappa coefficient, and IPTE. Given that the proposed method produces more accurate results by fusing two scale-change maps, it needs more computing time than the other methods used in this study. Therefore, the proposed method is efficient when accurate results are required, whereas the other methods used in this study should be selected for fast results.

4. Conclusion

This study develops an approach to change detection by fusing two change maps generated by an active contour model with different trade-off parameters. The experiments conducted on ETM+ and TM data sets confirm the effectiveness of the proposed approach. This work contributes to reducing the effect of the trade-off parameter μ on the change map, which makes the change map not only contain less false alarms but also retain accurate outlines of the changed regions. However, the values of the trade-off parameter μ are empirically selected in the traditional and proposed active contour approaches. Therefore, the automatic determination of the appropriate trade-off parameter must be investigated, and the proposed method must be applied to other types of remote sensing images in future work.

Acknowledgements

We thank the editor and referees for giving valuable suggestions that helped to significantly improve our article.

Disclosure statement

No potential conflict of interest was reported by the authors.

Funding

This work was supported in part by the Fundamental Research Funds for the Central Universities [grant number 2012LWB31]; and the National Natural Science Foundation of China [grant number 41331175]; a project funded by the Priority Academic Program Development of Jainism Higher Education Institutions.

References

Bazi, Y., F. Melgani, and H. D. Al-Sharari. 2010. "Unsupervised Change Detection in Multispectral Remotely Sensed Imagery with Level Set Methods." *IEEE Transactions on Geoscience and Remote Sensing* 48: 3178–3187. doi:10.1109/TGRS.2010.2045506.

Bruzzone, L., and D. F. Prieto. 2000. "Automatic Analysis of the Difference Image for Unsupervised Change Detection." *IEEE Transactions on Geoscience and Remote Sensing* 38: 1171–1182. doi:10.1109/36.843009.

Cao, G., Y. Z. Liu, and Y. F. Shang. 2014. "Automatic Change Detection in Remote Sensing Images Using Level Set Method with Neighborhood Constraints." *Journal of Applied Remote Sensing* 8: 083678. doi:10.1117/1.JRS.8.083678.

Celik, T., and K. K. Ma. 2011. "Multitemporal Image Change Detection Using Undecimated Discrete Wavelet Transform and Active Contours." *IEEE Transactions on Geoscience and Remote Sensing* 49: 706–716. doi:10.1109/TGRS.2010.2066979.

Chan, T. F., and L. A. Vese. 2001. "Active Contours without Edges." *IEEE Transactions on Image Processing* 10: 266–277. doi:10.1109/83.902291.

Chen, Y., and Z. G. Cao. 2013. "Change Detection of Multispectral Remote-Sensing Images Using Stationary Wavelet Transforms and Integrated Active Contours." *International Journal of Remote Sensing* 34: 8817–8837. doi:10.1080/01431161.2013.853145.

Hao, M., W. Z. Shi, H. Zhang, and C. Li. 2014. "Unsupervised Change Detection with Expectation-Maximization-Based Level Set." *IEEE Geoscience and Remote Sensing Letters* 11: 210–214. doi:10.1109/LGRS.2013.2252879.

Kass, M., A. Witkin, and D. Terzopoulos. 1988. "Snakes: Active Contour Models." *International Journal of Computer Vision* 1: 321–331. doi:10.1007/BF00133570.

Li, H., M. Gong, and J. Liu. 2015. "A Local Statistical Fuzzy Active Contour Model for Change Detection." *IEEE Geoscience and Remote Sensing Letters* 12: 582–586. doi:10.1109/LGRS.2014.2352264.

Lu, D., P. Mausel, E. Brondizio, and E. Moran. 2004. "Change Detection Techniques." *International Journal of Remote Sensing* 25: 2365–2401. doi:10.1080/0143116031000139863.

Osher, S., and J. A. Sethian. 1988. "Fronts Propagating with Curvature-Dependent Speed: Algorithms Based on Hamilton-Jacobi Formulations." *Journal of Computational Physics* 79: 12–49. doi:10.1016/0021-9991(88)90002-2.

Shi, J., J. J. Wu, A. Paul, L. C. Jiao, and M. G. Gong. 2014. "Change Detection in Synthetic Aperture Radar Images Based on Fuzzy Active Contour Models and Genetic Algorithms." *Mathematical Problems in Engineering* 2014: 1–15. doi:10.1155/2014/870936.

Shi, W. Z., and M. Hao. 2013. "A Method to Detect Earthquake-Collapsed Buildings from High-Resolution Satellite Images." *Remote Sensing Letters* 4: 1166–1175. doi:10.1080/2150704X.2013.858839.

Wu, Q. G., and J. B. An. 2014. "An Active Contour Model Based on Texture Distribution for Extracting Inhomogeneous Insulators from Aerial Images." *IEEE Transactions on Geoscience and Remote Sensing* 52: 3613–3626. doi:10.1109/TGRS.2013.2274101.

Yetgin, Z. 2012. "Unsupervised Change Detection of Satellite Images Using Local Gradual Descent." *IEEE Transactions on Geoscience and Remote Sensing* 50: 1919–1929. doi:10.1109/TGRS.2011.2168230.